J. Fluid Mech. (1988), *vol.* 191, *pp.* 419–442
Printed in Great Britain

Run-up of internal waves on a gentle slope in a two-layered system

By B. C. WALLACE AND D. L. WILKINSON
Water Research Laboratory, The University of New South Wales, Manly Vale, Australia

(Received 30 April 1985 and in revised form 2 November 1987)

This paper describes the dissipative phase of internal-wave run-up on uniform slopes of 0.030 and 0.054 rad as observed in a series of laboratory experiments. The waves were generated continuously at the interface of two miscible layers of differing density. As each wave in the perodic train propagated onto the slope, it steepened and developed into a solitary-like wave before finally overturning. Surrounding fluid was engulfed into the wave as it overturned and the resulting gravitational instability produced considerable turbulence and mixing. The broken wave took the form of a discrete bolus of dense fluid which propagated for some distance up the slope. Bulk parameters which characterize the nature of the bolus were defined and the dependence of these on the incident wave parameters and their behaviour during the run-up phase were examined.

1. Introduction

This paper describes an experimental study into the breaking and subsequent run-up of a continuous sequence of internal waves as they propagate onto a gentle slope [$\theta = 0.030$ and 0.054 rad (1.72° and 3.09°)]. Long internal waves were generated at the interface of a system initially composed of two miscible layers separated by a shallow halocline. The waves travelled for a distance of several wavelengths in water of uniform depth before encountering the slope. The nature of the breaking event and the subsequent wave run-up on the slope were examined in detail.

The experiments were intended to provide insight into the behaviour of a train of internal solitary waves as they travel shoreward from the shelf break onto a continental shelf. It is known that a variety of mechanisms exist which produce trains of internal solitary waves from interactions between the barotropic tide and bottom topography (Djorjevic & Redekopp 1978; Maxworthy 1980; Baines 1982). However the ultimate fate of these waves as they propagate shoreward across the shelf and finally dissipate their energy is not well understood.

Thorpe (1966) gave a qualitative description of some two-layer experiments in which interfacial waves shoaled onto a slope, and identified the dominant features of the run-up process. Thorpe observed that 'the front of the internal wave crest became almost distinct from the remainder of the (interfacial) profile and resembled a blob which travelled up the slope'. Dense fluid returning down the slope from previous waves appeared to flow over the top of the oncoming waves. This was attributed to mixing which occurred during the run-up phase and caused the return flow to be of an intermediate density.

Observations of internal-wave run-up in two-layered systems have also been reported by Hall & Pao (1969), Nagashima (1971), Southard & Cacchione (1972), Murota, Hirata & Michioku (1980), Kao, Pan & Renouard (1985) and Helfrich &

Melville (1986). Hall & Pao and Nagashima experimented with the shoaling and breaking of internal waves in immiscible two-layered systems. Hall & Pao measured wave energy spectra during shoaling and reported a transfer of energy to higher frequencies through growth of the harmonics. Nagashima was principally concerned with the reflection of internal-wave energy from a slope in an immiscible two-layered system. He found that on gentle slopes of less than about 15°, the reflection coefficient varied linearly with the slope inclination and decreased with increasing wave steepness. When the layers are miscible, dissipation appears to be more complete and Thorpe (1966) observed that 'very little wave energy was reflected from the slope'. Nagashima identified four modes of run-up: breaking, semi-breaking, wrinkle breaking (in which a train of interfacial capillary waves were observed to propagate away from the slope) and non-breaking. These modes, particularly the third, were strongly influenced by the small scale of the experiments and none was described in detail in the paper.

Southard & Cacchione (1972) conducted an experimental study of the shoaling and run-up of internal waves as a possible mechanism for the transport of sediment on a continental shelf. Their description of the run-up process was similar to that given by Thorpe (1966). They noted that the vortex of dense fluid (Thorpe's 'blob') which developed after the breaking event produced high velocities close to the bed and that sediment entrained into the vortex could be transported considerable distances up the slope.

Murota *et al.* (1980), Kao *et al.* (1985) and Helfrich & Melville (1986) have investigated the propagation and stability of internal solitary waves over slope–shelf topography. Evolution of the wave form was modelled both theoretically and experimentally. Close agreement was obtained for regions where the waves were weakly nonlinear. Helfrich & Melville found that if the local value of the ratio of wave height to lower-layer depth on the shelf was greater than about 0.35, kinematic instabilities produced a strong overturning which in some cases led to the generation of a second-mode wave at the pycnocline. For ratios of the wave height to the shelf depth of less than 0.30 no instabilities were observed, while for values between 0.30 and 0.35 they observed weak shearing instabilities. The varying ratios of wave height to lower-layer depth in Helfrich & Melville's experiments were made possible because of the presence of the shelf inshore from the slope. In the experiments described in this paper the depth reduced uniformly and only the strong overturning type instability (or wave breaking) was always observed.

Field observations of internal-wave breaking due to shoaling are relatively sparse. Emery & Gunnerson (1973) analysed bathythermograph data recorded in the 1950s on the continental shelf off Santa Monica. These records showed evidence of internal surf and swash. Seven classes of shoaling were identified ranging from no apparent shoaling effects to strong internal surf characterized by temperature inversions and isolated masses of cold water. Emery & Gunnerson (1973) used the term 'bolus' to describe these masses of denser water and the same term will be used here to describe the vortex of dense fluid which evolves from the overturning of an internal solitary wave.

Internal solitary waves have been observed by Osborne & Burch (1980) in the Andaman Sea and by Pingree & Mardell (1981) in the Celtic Sea. In both cases the waves were believed to have originated from the vicinity of the shelf break and the internal-wave packets showed consistent phasing with the barotropic tide. The observed celerity of the waves was in close agreement with the predicted speeds of internal solitary waves. In both of these studies the ratio of wave height to lower-

layer depth was less than 0.30 so that the overturning instability observed in various laboratory studies would not have yet developed (Helfrich & Melville 1986).

Haury, Briscoe & Orr (1979) in a study of the effects of internal waves on the distribution of plankton in Massachusetts Bay reported the existence of mixing across the thermocline on the western side of the bay where the internal waves shoaled and presumably broke. They found evidence of a turbulent outflow near the bottom, a characteristic feature of the run-up process described later in this paper and also noted in several of the previously cited references.

Recent studies of shelf processes in Bass Strait, which separates Tasmania from the Australian mainland, have revealed the presence of internal waves propagating normally onto the shelf from the shelf break. Continuous CTD profiling at a permanent station located approximately 10 km shoreward of the shelf break showed strong coherence between the internal waves and the M_2 tidal component (Jones & Padman 1983).

Figure 1 shows an isotherm pattern recorded in eastern Bass Strait in February 1984 during a period of strong internal-wave activity. The isotherms were interpolated from expendable bathythermograph casts which are shown as vertical lines in figure 1. The horizontal resolution is limited to one or two km and the detached vortex structures of the type described in this paper would not be resolved. However inspection of the 15° isotherm indicates appreciable run-up of cooler water onto the shelf. The vessel speed when these casts were taken was 43 km per hr which is much greater than the internal-wave celerity of about 1 km per hr. Consequently the isotherms in figure 1 can be regarded as being synoptic. Simultaneous temperature and salinity profiles recorded from a fixed platform located in 83 m of water approximately 10 km to the west of the vessel verified that the waves were propagating normally to the bottom contours. Density differences due to variation of salinity over the depth were negligible compared with those due to temperature.

The experiments described in this paper are only relevant to situations where the vertical density structure may be reasonably approximated by two layers separated by a relatively thin thermocline. When the density stratification is continuous over the depth, the nature of the internal waves is quite different and wave energy is transmitted along inclined rays whose slope is determined by the ratio of the wave frequency to the buoyancy frequency. These internal waves can only propagate onto a slope if the ray inclination is less than that of the slope, otherwise the internal waves are reflected back into deeper water. Cacchione & Wunsch (1974) have convincingly demonstrated these processes in laboratory experiments. Eriksen (1982) has observed strong perturbations to the internal-wave spectrum at sites above sloping bottoms in the Atlantic Ocean, and attributes these to reflection of internal waves by the slope.

Continuous stratification is more applicable to wintertime conditions, and to waters below the thermocline and generally below the shelf break. The two-layer approximation is, however, not an unrealistic representation of the summer thermocline and the two-layer situation examined in this paper may apply to internal waves propagating on the thermocline onto a continental shelf.

The experimental facility and the manner in which the experiments were conducted are described in §2.1. This is followed in §2.2 by a description of the shoaling and overturning of an internal wave and evolution of the bolus in a typical experiment. In §3 the relationship between the characteristic parameters of the incident wave and the resulting bolus are examined and a model is presented which quantifies the behaviour of the bolus as it travels up the slope.

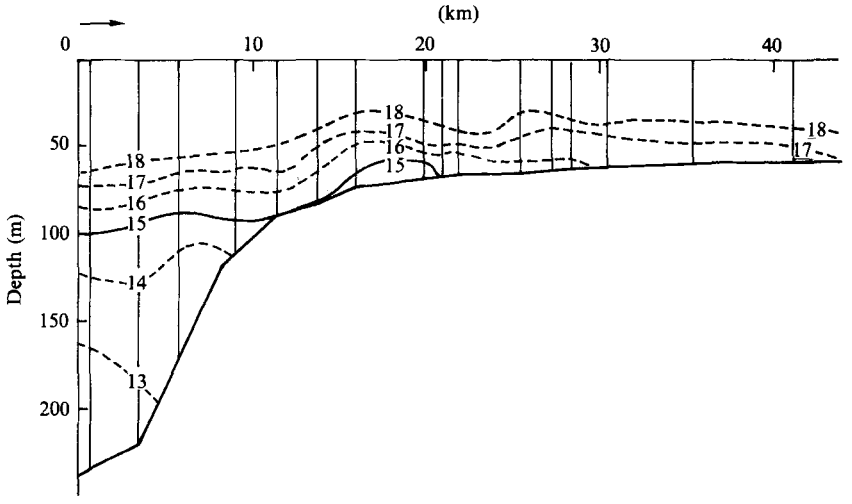

FIGURE 1. Thermal structure along a section normal to the shelf in eastern Bass Strait. The vertical lines indicate sites where temperature sections were taken.

2. Experiments

2.1. *The facility and experimental technique*

The experiments were performed in an articulated tank, 18 m long, 600 mm wide and 750 mm deep. The depth in the tank was uniform for 12 m and thereafter reduced uniformly as shown in figure 2. An internal-wave generator, located at the end of the tank, produced internal waves which propagated towards the slope. The tank was filled with fresh water to a depth of approximately 370 mm and then a brine solution was slowly injected beneath the lighter fresh water until the bottom layer was approximately 130 mm deep. The thickness of the halocline between the layers was typically 15–30 mm and the vertical density profile could be closely approximated by a hyperbolic tangent. The difference in the relative densities of the two layers ranged from 0.013 to 0.051 in the different experiments. Withdrawal syphons were provided at the level of the interface to enable it to be sharpened, if necessary. This allowed several experiments to be performed sequentially without replacing the layers. The syphons were removed prior to the commencement of an experiment. It was subsequently found that the nature of the internal-wave run-up was relatively insensitive to the initial thickness of the halocline.

The internal waves were generated by a horizontal paddle which pivoted about its forward edge. A bulbous nose attached to the forward edge prevented overturning and mixing in the halocline adjacent to the paddle. The oscillating rear end of the paddle slid against a cylindrical back stop which prevented exchange and mixing between the layers at the paddle. The paddle was driven by means of a crank arm attached to a variable-speed drive unit and an electric motor, and could produce waves with periods between 5 and 20 s. The stroke of the crank arm could be adjusted to vary the height and steepness of the internal waves.

The structure of the internal waves during the shoaling and run-up phases was determined by means of conductivity probes from which the density structure could be evaluated, and also by various flow-visualization techniques which included the use of refraction screens, dye injection and the tracking of neutrally buoyant particles.

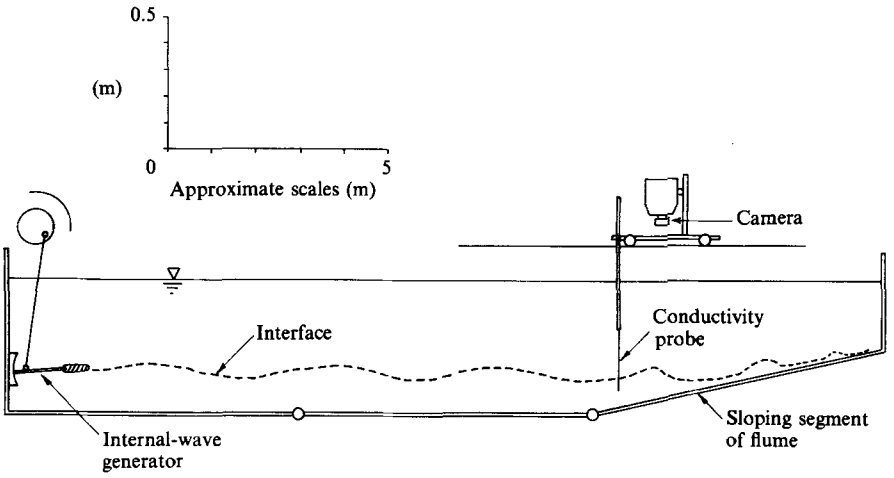

FIGURE 2. Schematic diagram of the experimental facility.

The conductivity probes were based on a design described by Alonso (1971). The sensor consisted of two platinumized gold electrodes, each 2 mm long and spaced 1.5 mm apart. The finite size of the probe limited spatial resolution of structure to about 5 mm and the system response was limited to frequencies below 10 Hz. The probes were adequate to record the mean density structure of the internal waves but their ability to resolve turbulence was limited.

Refraction screens were used extensively to visualize the gross features of the wave run-up. The refraction screen consisted of a series of fine diagonal lines drawn on a white screen. Wave-induced mixing and displacement of pycnoclines produced by the internal waves caused variations in refractive index which gave a distorted image of the refraction screen when viewed through the tank. The technique provided a clear indication of the wave structure and also of any mixing that occurred.

During the later stages of wave run-up the broken wave front was slightly retarded at the sides of the tank owing to frictional effects. The three-dimensionality of the flow close to the walls prevented effective use of the normal shadowgraph technique. However this difficulty was resolved by inserting a moveable refraction screen about one-third of the way across the tank and viewing it from above using an inclined mirror located about one-third of the tank breadth from the opposite side. The installation is shown schematically in figure 3. The refraction screen was viewed through the middle third of the tank where the mean flow was essentially two-dimensional. The mirror and the screen were 400 mm long and 250 mm high and were carefully aligned parallel to the axis of the tank. The mirror and screen could be moved to any desired location along the tank. Although the inclined mirror and to a lesser extent the vertical screen produced some localized disturbance to the flow, because of their limited extent the regions affected by their presence were a small fraction (less than 10%) of the viewing distance between them. This was confirmed by tracking neutrally buoyant particles at different positions between the mirror and the screen. Trial experiments with the screens removed showed no detectable changes to the structure (as measured by conductivity probes) or celerity of the wave. The inclined mirror and an alternate screen marked with a rectangular grid were used to observe the motion of neutrally buoyant particles and dye traces. These motions were recorded photographically using either motion-picture film or by

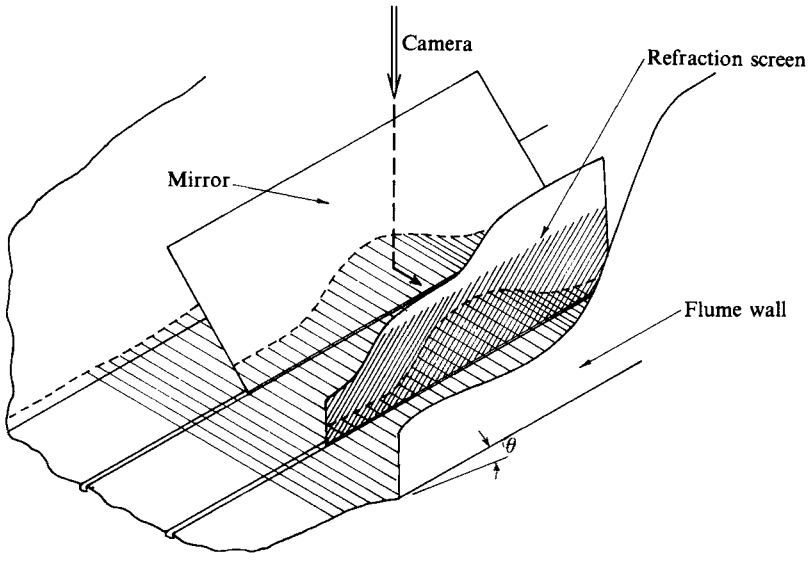

FIGURE 3. Technique employed to photograph the bolus.

means of multiple exposures on a single frame using a stroboscopic flash unit. The latter technique proved to be less time consuming for deduction of velocities and pathlines in the flow. The mirror enabled particles to be viewed simultaneously from above and from the side. Only particles well removed from the mirror and the screen were selected for quantitative velocity evaluations.

The wave celerity in the constant-depth section of the tank was measured by timing the transit of the wave crest between conductivity probes placed about a half-wavelength apart. Measurements in one experiment at several different locations along the constant-depth section of the tank showed that the wave celerity was constant in this region. These records were also used to measure reflection of wave energy from the slope; however a reflected wave was not detected, indicating that its height was less than 3% of the incident-wave height. This figure was based on the resolution of the conductivity probes at the wave frequency.

Numerous repetitions of a single set of experimental conditions were required to resolve the structure of the breaking process and subsequent run-up. For this reason only six different experiments were performed in all, five on a slope of 0.030 rad and one on a slope of 0.054 rad. The steepness of the internal waves in the constant-depth region of the tank was varied between 0.0019 and 0.0084 in the different experiments. The ratio of the effective layer depth d, defined as $d = d_u d_\ell/(d_u + d_\ell)$ where d_u and d_ℓ are the depths of the upper and lower layers respectively, to the wavelength ranged from 0.024 to 0.083. Table 2 in Appendix A summarizes the properties of the waves in the constant-depth section of the tank while the characteristics of the breaking and run-up phase are given in table 3 in Appendix A.

2.2. *Evolution and run-up of the bolus*

The shoaling, breaking and run-up of internal waves in a typical experiment (no. 4, see tables 2 and 3 in Appendix A) are now described. The bottom layer in this experiment consisted of a brine solution having a density of 1051 kg m^{-3} and was 130 mm deep at the generator end of the tank. The upper layer was fresh water and

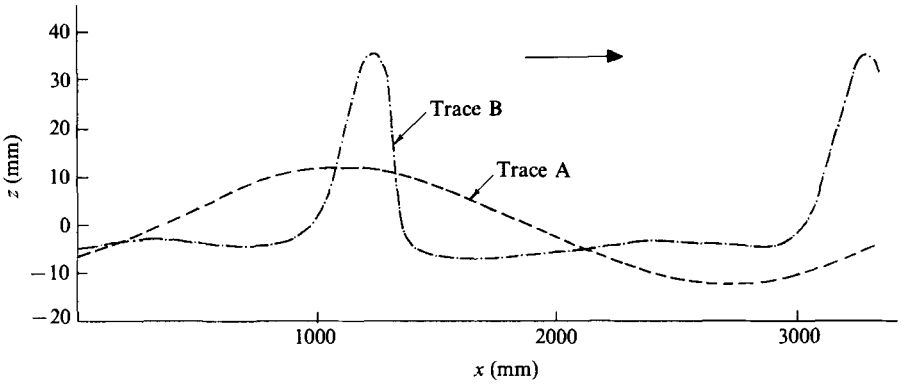

FIGURE 4. Conductivity traces from the constant-depth region of the tank (A) and on the shelf just prior to breaking (B).

was 370 mm deep. The halocline separating the layers had a thickness of about 20 mm.

The period of the internal waves was 18.9 s and their wavelength was 3650 mm at the generator end of the tank where the depth was uniform. The vertical extent of particle excursion in the halocline was 21 mm and this was taken to be the height of the incident internal wave. Only first-mode oscillations were observed and no reflections from the slope could be detected. The distance between the internal-wave generator and the toe of the slope was 12 m and the slope inclination was 0.030 rad.

Oscillations of the halocline were very nearly sinusoidal in the section of the tank where the depth was uniform as indicated by trace A in figure 4, which is based on the record from a conductivity probe sited at the inflexion point of the halocline. Conductivity variations were transformed into vertical displacements using the initial vertical salinity distribution recorded prior to the waves being generated. The record provided an indication of vertical movements induced by the waves. Note the near symmetry of the wave crests and troughs about the mean level. Trace B in figure 4 shows a similar record based on the output of a conductivity probe located 3200 mm upslope from the toe of the slope where there is a gross change in the wave form with a marked steepening of the crest and flattening of the trough. The nearly sinusoidal waves observed in the constant-depth region of the tank evolved into a train of solitary waves as they progressed onto the slope.

The waves continued to steepen until they became unstable and overturned. This process is shown in figure 5 where the waves are travelling from left to right up the slope. A refraction screen is viewed through the waves and gives an indication of the wave form. Where fine structure produced by turbulence is present, the screen is obliterated. The grid in these photographs has a spacing of 100 mm between normals to the slope and 50 mm between grid lines parallel to the slope. The sequence of events shown in figures 5, 6 and 7 only evolves after several waves have progressed onto the slope. The first few waves behave differently and are discussed later.

Figure 5(*a*) shows the last stages of wave steepening. Ahead of the wave is a thin layer of backflow from previous waves. The next photograph in the sequence, 5(*b*), taken 0.5 s later (corresponding to $0.026T$ where T is the wave period) shows an instability which developed in the region of high shear near the wave crest. Figure 5(*c*) shows the wave a further 0.5 s later where overturning of the wave is clearly

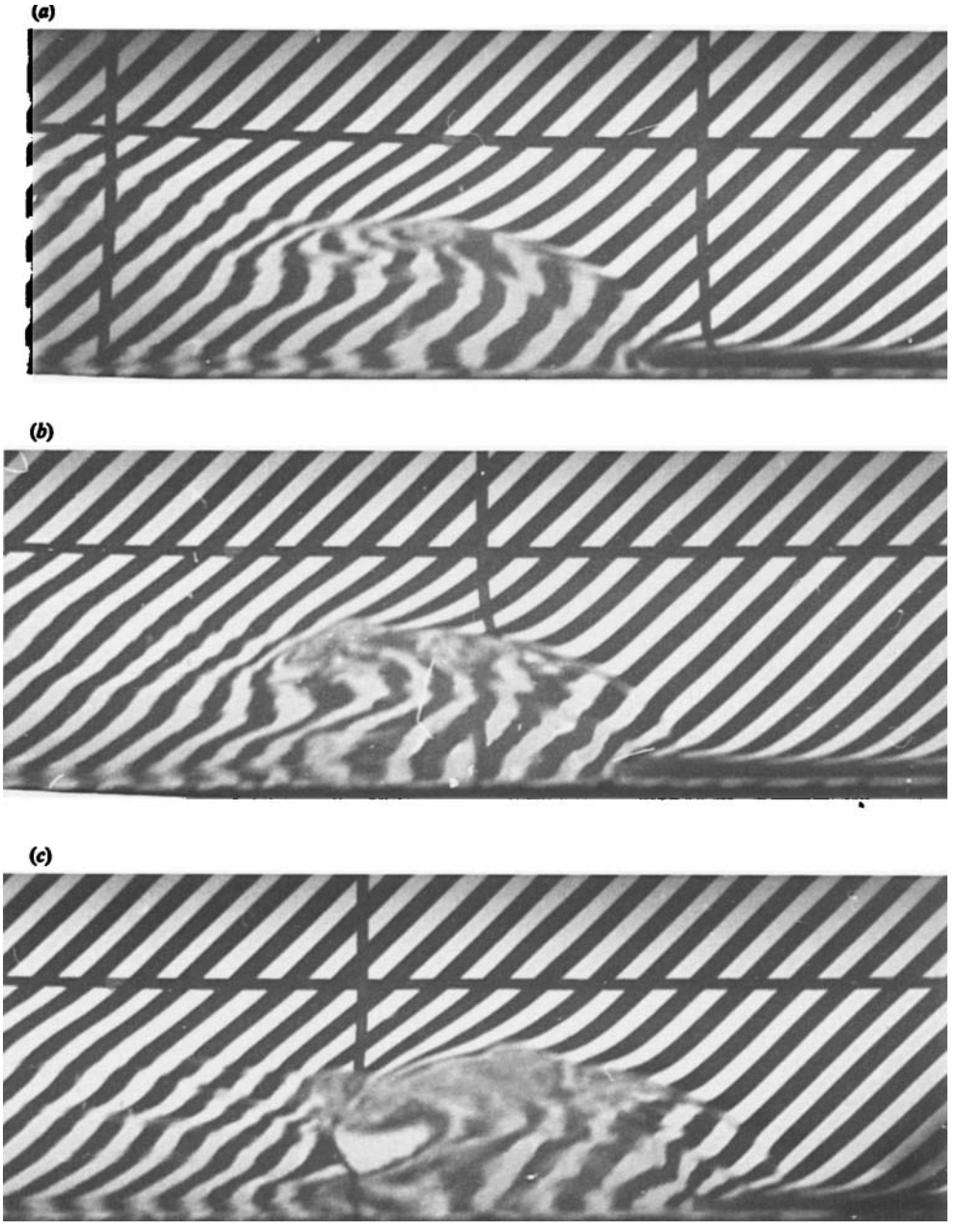

FIGURE 5. Sequence of photographs showing the internal wave immediately prior to and at overturning. The wave is travelling from left to right in the upslope direction.

visible. This overturning is a striking characteristic of the breaking process and was first reported by Thorpe (1966). The backflow, which because of mixing which occurred later in the run-up process, was of a density intermediate between that of the upper and lower layers. The backflow was therefore carried up and over the approaching waves. During the overturning event which resulted in the formation of the bolus, there was appreciable engulfment of fluid from the backflow into the

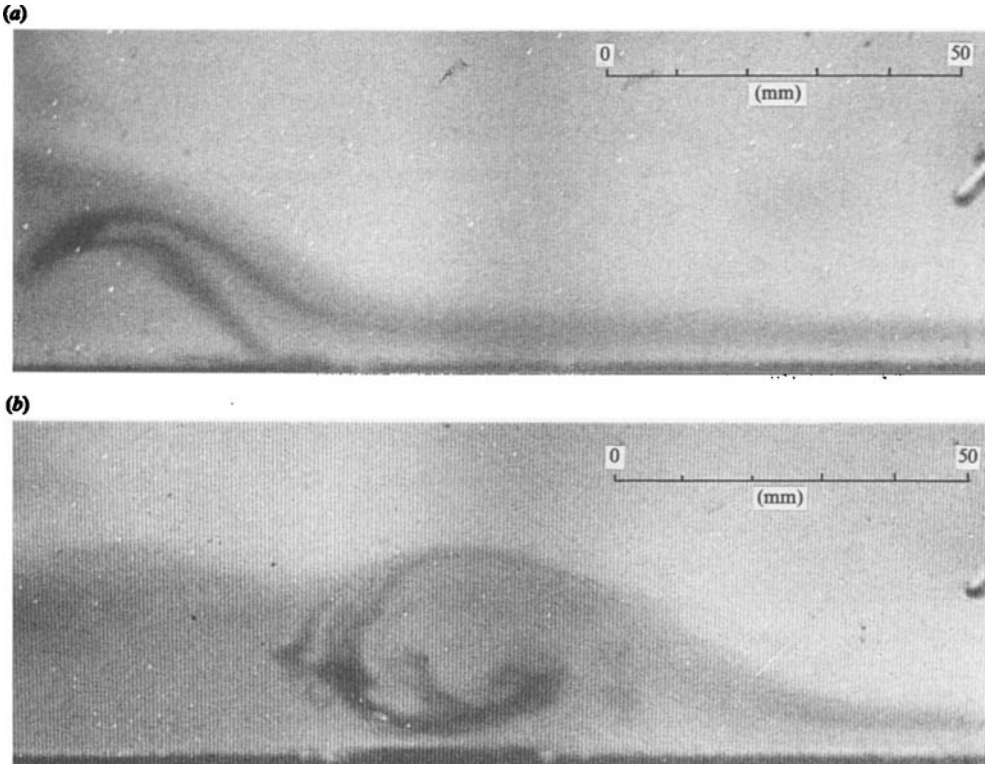

FIGURE 6. Dye streaks in the backflow showing the engulfment process that accompanies the overturning event. The wave is travelling from left to right in the upslope direction.

overturning wave. This can be seen in figure 6 where dye was injected into the backflow and its incorporation into the overturning wave is clearly evident. The two dye streaks visible in the figure originated from two different levels of dye injection within the backflow. The timing of figures 6(*a*) and 6(*b*) corresponded exactly to that in figures 5(*b*) and 5(*c*). The camera position remained unchanged between the two photographs in figure 6 and the forward advection of the dye with the breaking wave gives a clear indication of the up-slope mass transport. The dye patch was subsequently mixed by turbulence within the bolus and was carried with it up the slope.

It will be noted that up to the stage shown in figures 5(*c*) and 6(*b*) the motion had been largely non-turbulent. The overturning produced a gravitational instability and intense mixing which continued as the bolus travelled up the slope. The structure of the bolus was quite different from the solitary wave from which it evolved. This is clearly evident in figure 7 (*a–c*) which continues the sequence begun in figure 5. Figure 7(*a*) was taken 1.5 s (0.08T) after figure 5(*c*). Fine turbulent structure inside the bolus has obliterated the refraction screen. Dense fluid was observed to drain from the rear of the bolus causing its size to slowly diminish as it progressed up the slope. The frontal shape of the bolus was similar to the surge fronts described by Wood & Simpson (1984) in their study of the propagation of internal surges. The front of the bolus was remarkably two-dimensional, as was also observed in internal surges. Evidently the presence of a dense bottom layer ahead of a front (the backflow in the case of a bolus) suppressed the lobe-and-cleft formation seen at the front of gravity

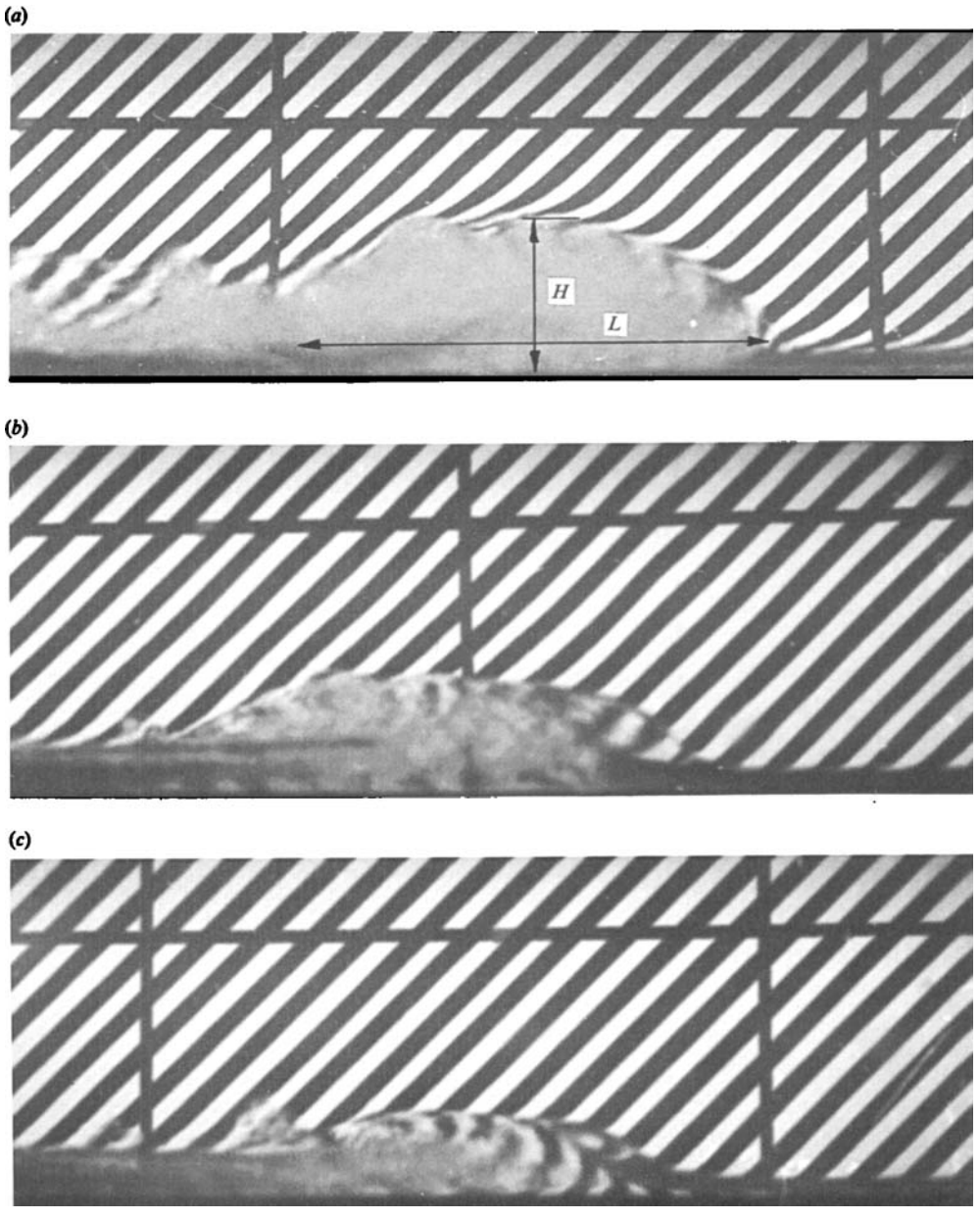

FIGURE 7. Run-up of the bolus after the overturning event. The bolus is travelling from left to right in the upslope direction.

currents (Simpson 1972). Only close to the sidewalls did viscous effects cause a retardation of the bolus but elsewhere (for a distance of at least ten bolus heights across the tank) the structure was strongly two-dimensional. The shape of the bolus did not change appreciably as it travelled up the slope, as can be seen in figure 8 where the ratio of the height of the bolus H to its length L is shown at various stages of run-up. The measurements of height and length were based on the extent of fine structure as indicated in figure 7(a). The ordinate scale in figure 8 is the distance x between the bolus and its limit of run-up normalized by the total run-up distance

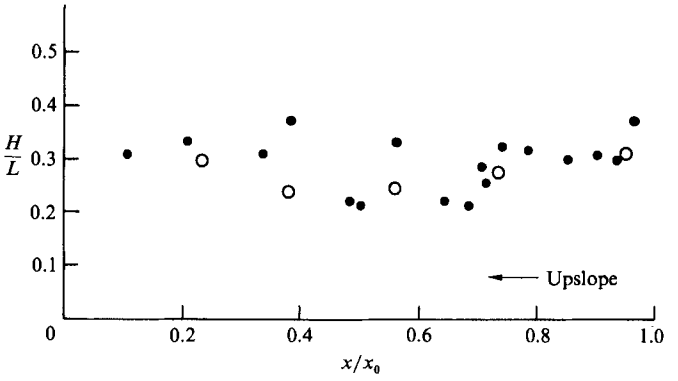

FIGURE 8. The bolus height-to-length ratio as a function of the normalized distance from the limit of run-up. Bedslope: ●, $\theta = 0.030$; ○, $\theta = 0.054$.

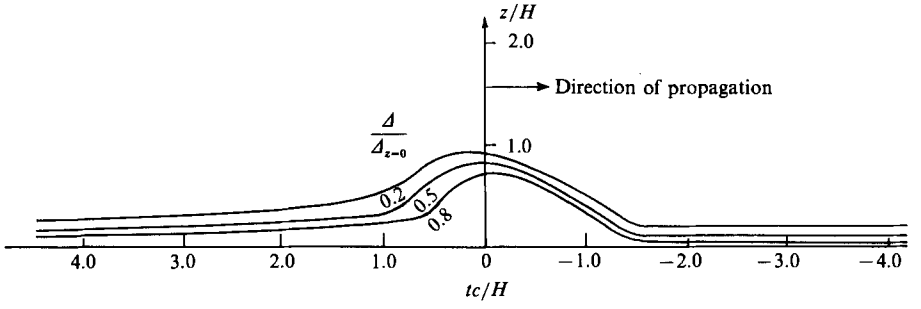

FIGURE 9. The mean density structure of the bolus (the normalized timescale on the abscissa axis is the equivalent of the lengthscale on the ordinate axis).

x_0 as indicated in the figure. There is no systematic variation in the ratio H/L during run-up and this self preserving property of the bolus is employed in the later analysis.

The density structure of a bolus is shown in figure 9 where the local density excess Δ has been normalized with respect to the local maximum. Figure 9 was deduced from time series recorded by stationary conductivity probes located at nine equally spaced levels over the height of the bolus. The time series on the abscissa axis has been converted to a spatial scale equivalent to that used on the ordinate axis by normalizing with respect to bolus height H and local celerity c. The bolus shown in figure 9 can be regarded as advancing from left to right. Note the steep density gradient at the forward face of the bolus and the large region of essentially homogeneous fluid within the core. A turbulent weakly stratified wake existed behind the bolus. The conductivity probes were functioning near the limit of their resolution at the front of the bolus. Interpretation of the density structure in this region was assisted by tracking neutrally buoyant particles in the backflow and in the core of the bolus.

Figure 10 shows a schematic representation of the structure of a bolus as seen by an observer moving with it. The structure was deduced from the conductivity measurements and from analysis of motion-picture film on which the movements of dye streaks and neutrally buoyant particles were recorded. The bolus contained a well-mixed core and measurements indicated that velocities of circulation within the core were comparable with the celerity of the core itself. The circulation coupled with

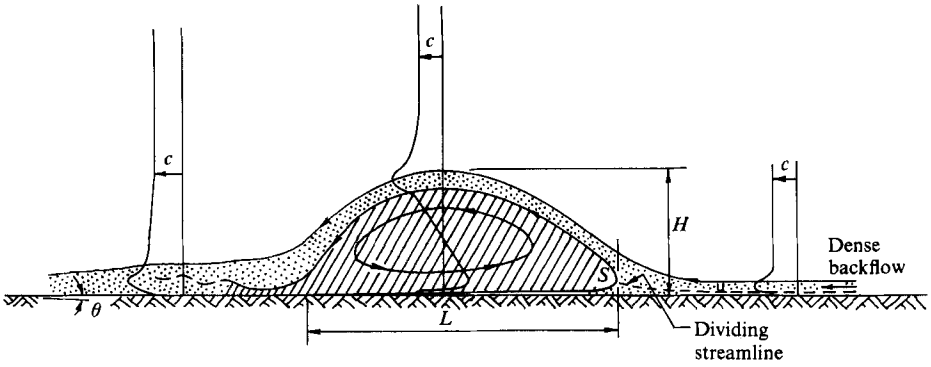

FIGURE 10. The structure of the bolus as seen by an observer moving with the same speed. The mean distributions of the horizontal velocity component are shown at sections ahead of, through and behind the bolus.

the forward speed of the bolus produced high velocities close to the bed thereby enhancing the capacity of these structures to entrain and transport bottom sediments in the manner described by Southard & Cacchione (1972). It was not the intention of this study to describe the internal structure of the bolus in great detail but rather to examine the behaviour of its bulk parameters as it propagated up the slope.

The backflow is an important feature of the run-up phase and is clearly visible adjacent to the bed both ahead of and behind the bolus in figures 5 and 7. The velocity of the backflow was primarily determined by gravity and friction, and on the mild slopes employed in these experiments interfacial mixing was suppressed by buoyancy effects. When the backflow reached the level of the original halocline it formed a thin intrusive layer which slowly grew out from the slope along the original interface. Ultimately the presence of this layer must modify the approaching waves; however the experiments were not of sufficient duration for this to be of measurable significance.

The interaction between the first few waves and the slope, after the wave generator was started, was very different from that which developed later and has already been described. The initial waves were of a lesser height, with the wave height increasing almost linearly for the first four or five waves after which a quasi-steady state became established. Figure 11 shows the run-up of the second wave front in a train of solitary waves. The dramatic overturning did not develop and the wave front simply surged onto the slope with minimal mixing. The elevation of the limit of run-up was comparable with the elevation of the incident wave crest; however, because of the smaller wave height, the run-up distance was appreciably less than that of subsequent waves.

The weakness of the backflow from these initial waves is believed to be a significant factor affecting their run-up and the absence of the initial overturning.

Although the run-up phase in these experiments differed from that described by Kao *et al.* (1985) and by Helfrich & Melville (1986) where the slope terminated at a horizontal shelf, the overturning observed in some of their experiments was similar to that described here. The difference in behaviour after breaking was presumably due to the different bottom geometry used in this study. Helfrich & Melville (1986) reported that fluid mixed during the breaking event propagated across the shelf as a second-mode internal solitary wave. The wave contained regions of closed

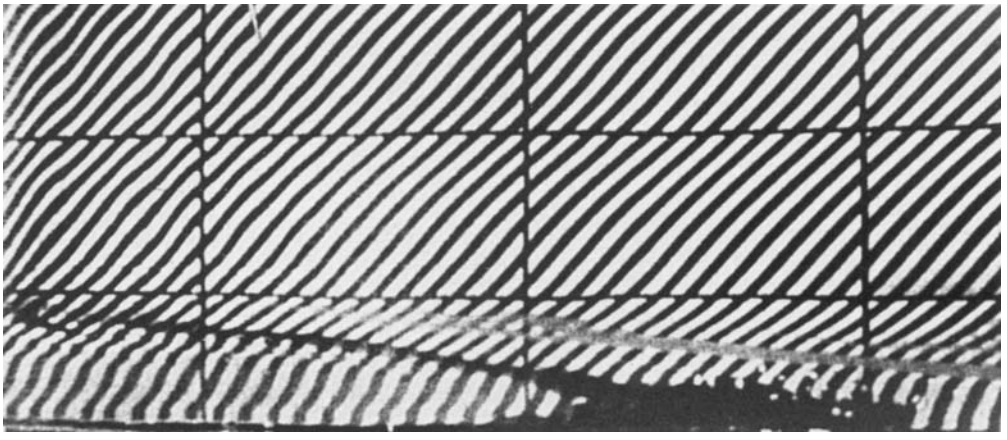

FIGURE 11. Run-up of the second wave in a train of solitary waves. The wave front is travelling from left to right in the upslope direction.

circulation not unlike that described by Davis & Acrivos (1967) in their study of second-mode solitary waves at the interface of two deep layers.

Peregrine (1974) has described a homogeneous free-surface flow which is remarkably similar in form to the boluses described here. The phenomenon, which Peregrine referred to as a shear wave, is sometimes observed in the backflow from surf on a beach and consists of hydraulically supercritical flow over a separation eddy. In an elegantly simple analysis Peregrine showed that the form of the shear wave is determined by the Froude number of the backflow relative to the wave. It might be expected that the form of the bolus would show a similar dependence on the backflow which in turn would depend on the bed slope.

3. Model of bolus run-up

The propagation of a long interfacial wave onto a gentle slope consisted of two phases. The first was a conservative shoaling phase in which the motion in each layer was essentially irrotational. As the effective depth decreased the wave steepened and ultimately instabilities produced an overturning which resulted in the formation of a turbulent bolus. A dissipative phase followed in which the bolus progressed up the slope, slowly losing momentum and diminishing in size as it gained elevation.

In this section the relationship between the parameters that characterize the incident wave and those that characterize the bolus that evolves from it are examined. This is followed by a description of a model for the dissipative phase of bolus run-up.

3.1. *Shoaling of the internal wave*

Interfacial waves in a system consisting of two layers can be described in terms of the following conservative properties: the energy flux P, the wave period T and length of the wave λ_0 if the upper and lower layers were infinitely deep. These three parameters characterize the wave for any value of the effective depth d, as previously defined. The energy flux can be evaluated at any convenient location from the relationship

$$P = \tfrac{1}{2}\Delta g a^2 c_g, \tag{1}$$

where Δ is the difference in relative density of the layers, g is gravitational

acceleration, a is the local amplitude of the internal wave and c_g its local group velocity. The reference wavelength is given by

$$\lambda_0 = \frac{\Delta g T^2}{2\pi} \tag{2}$$

and defines a characteristic lengthscale of the wave. These conservative wave parameters yield a single non-dimensional parameter $P^* = PT^3/\lambda_0^4$ which characterizes a particular wave and is independent of the local depth. It follows therefore that the properties of the bolus when it first evolves after the overturning event, for example its height H_0 relative to the characteristic lengthscale of the wave is determined by P^* and the slope inclination θ.

Indeed such a relationship is known to exist for shoaling surface waves where the ratio of the wave height at breaking to the wavelength in deep water is a function of the deep-water-wave steepness and the beach slope (Goda 1970). It can be shown for surface gravity waves that P^* is proportional to the square of the deep-water-wave steepness (Appendix B).

Figure 12 shows the initial height of the bolus H_0 normalized with respect to λ_0 as a function of P^* for each of the experiments. The height of the bolus was taken to the limit of fine structure as indicated in figure 7 (a). The straight line in figure 12 has a slope of $\frac{1}{3}$ and corresponds to the power law first obtained by Munk (1949) relating the steepness of a surface gravity wave in deep water to the normalized breaking height of the wave as it shoaled. This dependency was obtained by equating the energy of a small-amplitude wave in deep water to the energy of a solitary wave of limiting height in shallow water. No attempt was made to match coefficients in figure 12 because the two breaking mechanisms appear quite different. However the trend of the data, although limited, suggests that shoaling internal waves show a similar dependence on P^*.

It was seen in figure 6 that as the wave overturned backflow was drawn into the wave causing the mean density excess in the resulting bolus, Δ_0, to be less than the density excess in the lower layer away from the shoaling region, Δ_ℓ. The ratio Δ_0/Δ_ℓ, which is a measure of the fraction of fluid from the denser layer in the bolus when it first forms, is plotted against P^* in figure 13. Surprisingly Δ_0/Δ_ℓ increases with P^*, indicating that the engulfed fraction decreases as the characteristic energy flux becomes larger. The energetics of breaking surface waves show a similar trend. Breaking occurs in a gentle spilling mode when the deep-water-wave steepness ($\sim P^{*\frac{1}{2}}$) is large, and more violently in a plunging mode with much mixing and turbulence when the deep-water steepness is small (Goda 1970). Although these experiments suggest that internal waves break in an entirely different manner to surface waves, the intensity of the breaking event shows a similar trend with increasing values of P^*.

The location of the point where overturning occurred was also of interest and was found to be just downslope from the intersection of the halocline with the slope, in the absence of waves. The ratio of the lower-layer depth (without waves) at the point of overturning, d_0, to the height of the resulting bolus H_0 was found to be 0.22 ± 0.13. There was no systematic variation of this ratio with P^* and the large variance of the ratio is consistent with difficulties in defining a precise break point.

3.2. *Bolus run-up*

Having established the relationship between the parameters characterizing the initial bolus and the incident wave, a simple model is presented which describes the

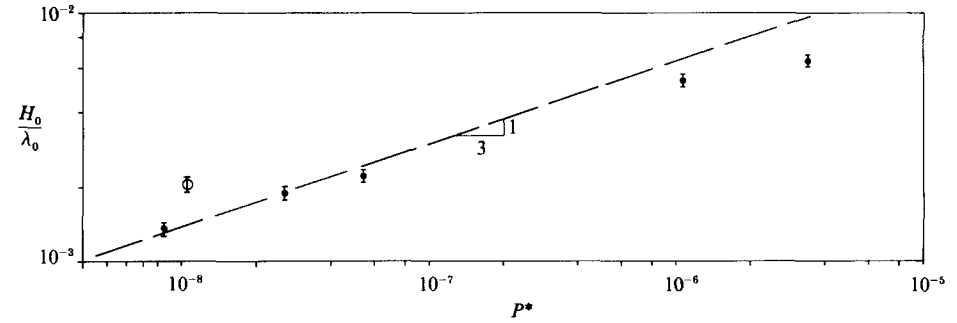

FIGURE 12. Ratio of initial bolus height to the characteristic wavelength H_0/λ_0 as a function of the characteristic energy flux P^*. Bedslope: ●, $\theta = 0.030$; ○, $\theta = 0.054$.

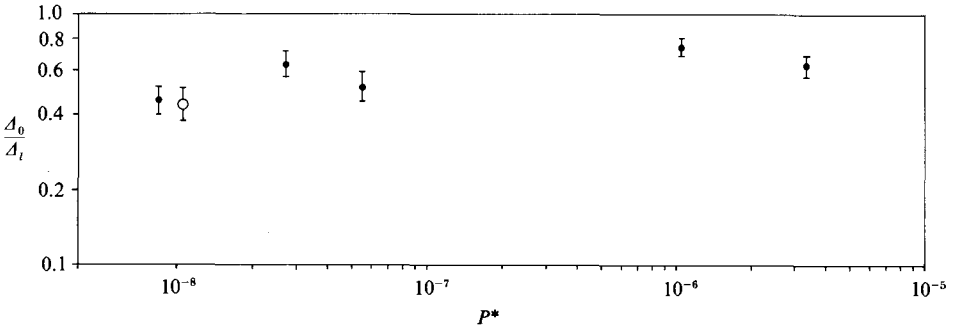

FIGURE 13. Ratio of the density excess of the initial bolus to the density excess of the lower layer (Δ_0/Δ_ℓ) as a function of the characteristic energy flux P^*. Bedslope: ●, $\theta = 0.030$; ○, $\theta = 0.054$.

variation of speed c, height H and density of the bolus as it travels up the slope. A characteristic density excess Δ was defined as the ratio of the mean density excess within the core of the bolus (taken as the region containing fine structure) to the density of the upper layer. It is assumed that $\Delta \ll 1$ so that density variations are only accounted for in gravitational terms.

It was noted in §2 that once a bolus formed, its shape remained unchanged as it travelled up the slope. Confirmation of this observation was provided in figure 8. Preservation of form has clear implications as regards the dynamics of the bolus. Consider the schematic diagram of a bolus shown in figure 10. A stagnation point must exist at some location S in the vicinity of the nose and the dynamic pressure there, p_s, scales as

$$p_s \sim \tfrac{1}{2}\rho c^2,$$

where c is the celerity of the bolus and ρ is the fluid density. p_s is matched by an equal pressure at the same point on the interior of the bolus. If it is assumed that the circulation velocities within the bolus are proportional to c, which is consistent with the self-similar form of the bolus, then the interior pressure at S scales as

$$p_s \sim \Delta\rho g H - \psi\tfrac{1}{2}\rho c^2,$$

where g is gravitational acceleration and ψ is a dimensionless constant whose value depends on the flow pattern within the bolus. When the two expressions for p_s are equated a bolus Richardson number defined by $R_i = \Delta g H/c^2$ is given by

$$R_i = \tfrac{1}{2}(1+\psi). \tag{3}$$

Thus if the form of the bolus is unchanging, its dynamic structure, characterized by R_i, is also preserved.

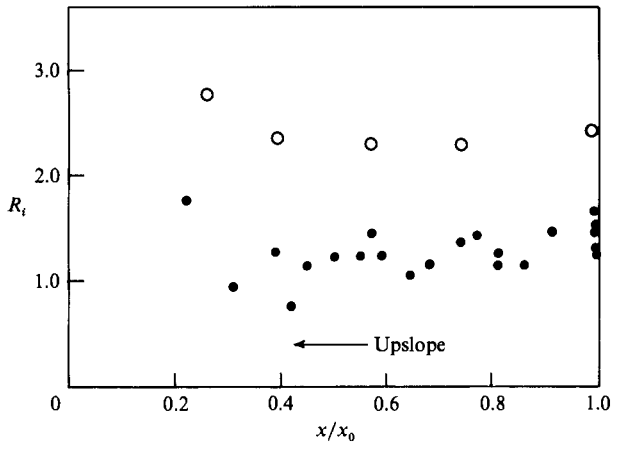

FIGURE 14. Bolus Richardson number as a function of the normalized distance from the limit of run-up. Bedslope: ●, $\theta = 0.030$; ○, $\theta = 0.054$.

The validity of these arguments is tested in figure 14 where locally determined values of the bolus Richardson number are shown at various stages of run-up. Although there is considerable scatter in the data there appears to be no systematic variation of the Richardson number during the run-up phase. The variance ratio for the data on the slope of 0.030 amounts to 35%; however this is quite consistent with the variances of about 8% in Δ, H and c. The increased scatter at small values of x/x_0 near the limit of run-up was caused by difficulties of measurement when the bolus had diminished to a small size. The mean value of the bolus Richardson number was 1.27 ± 0.34 on the slope of 0.030 and 2.4 ± 0.3 on the slope of 0.054. No systematic variation of R_i with the characteristic energy flux P^* was detected, indicating that the structure of the bolus is determined by the inclination of the slope and is independent of the nature of the breaking event.

The bolus when it first formed possessed forward momentum; however gravitational forces acting back along the slope, and fluid drag and momentum imparted by the backflow from preceding boluses progressively reduced the momentum of the bolus as it travelled up the slope. The local force balance can be expressed in terms of the previously defined bulk parameters and is given by

$$\frac{\mathrm{d}}{\mathrm{d}t}[S_1 \rho(1+k_v) cH^2] = -S_1 \Delta \rho g H^2 \sin\theta - C_D H \rho c^2 - C_m \frac{\rho q^2}{h}. \tag{4}$$

The bracketed term on the left-hand side of (4) is the momentum of a two-dimensional bolus. S_1 is a dimensionless shape factor such that $S_1 H^2$ expresses the cross-sectional area of the bolus, and k_v is an added-mass coefficient accounting for motion induced by the bolus in the surrounding fluid. θ is the inclination of the slope. The first term on the right-hand side of (4) is the downslope component of the submerged weight of the bolus. The next term is the drag force where the drag coefficient C_D is based on the height and speed of the bolus. The last term is the momentum imparted to the bolus from the backflow where C_m is a momentum-transfer coefficient, q is the two-dimensional volume flux and h the depth of the backflow.

Continuity considerations require that the mean upslope transport by the boluses is balanced by the downslope transport in the backflow. It follows therefore that

$$q \sim \frac{S_1 H^2}{T},$$

where T is the period of the incident waves. Some terms in (4) are more important than others and with the intention of simplifying the equation, the magnitudes of the different forcing terms are examined. If the right-hand side of the momentum equation is normalized by dividing through by $\rho c^2 H$, the forcing terms can be expressed as

$$-S_1 R_i \sin\theta - C_D - C_m S_1^2 \frac{H}{h}\left(\frac{H}{cT}\right)^2.$$

On slopes where $\sin\theta = O(10^{-2}\ to\ 10^{-1})$, the magnitudes of the forcing terms are to be found to be 10^{-1}, 10^{-1} and 10^{-2} respectively. Thus as a first approximation, the momentum contributed from the backflow can be neglected. Only when $H/cT > 10^{-1}$ does the last term in (4) become significant. It is uncertain whether internal waves of such steepness would behave in the manner observed in the experiments, where H/cT was $O(10^{-2})$.

Equation (4) can be expressed more conveniently in a spatial frame in which $H(t)$ is replaced by $H(x)$ and the origin of x is located at the limit of run-up with the x-axis directed back down the slope as shown in figure 10. The celerity of the bolus in this frame is given by

$$\frac{\mathrm{d}x}{\mathrm{d}t} = -c, \tag{5}$$

and the equation of motion then becomes

$$c\frac{\mathrm{d}}{\mathrm{d}x}[S_1 \rho(1+k_v)\, cH^2] = S_1 \Delta\rho g H^2 \sin\theta + C_D H\rho c^2, \tag{6}$$

where only the dominant terms have been retained.

Now if $\Delta\rho g H$ in the first term on the right-hand side of (6) is expressed in terms of the bolus Richardson number the following results:

$$S_1(1+k_v)\frac{\mathrm{d}}{\mathrm{d}x}(cH^2) = (S_1 R_i \sin\theta + C_D)\, cH. \tag{7}$$

The self-preserving nature of the flow implies that the variables that characterize the bolus can be expressed as powers of x and for (7) to be dimensionally homogeneous H must have a linear dependency on x. Thus if the bolus is first identified at a location x_0, where its height is H_0, then its height H at any point x further up the slope is given by

$$\frac{H}{H_0} = \frac{x}{x_0}. \tag{8}$$

Elimination of H between (7) and (8) gives, after some manipulation,

$$x\frac{\mathrm{d}c}{\mathrm{d}x} = \left[\left(\frac{x_0}{H_0}\right)\left(\frac{S_1 R_i \sin\theta + C_D}{S_1(1+k_v)}\right) - 2\right]c. \tag{9}$$

When (9) is integrated between the reference position and an intermediate point of run-up, the following results:

$$\frac{c}{c_0} = \left(\frac{x}{x_0}\right)^{\phi}, \tag{10}$$

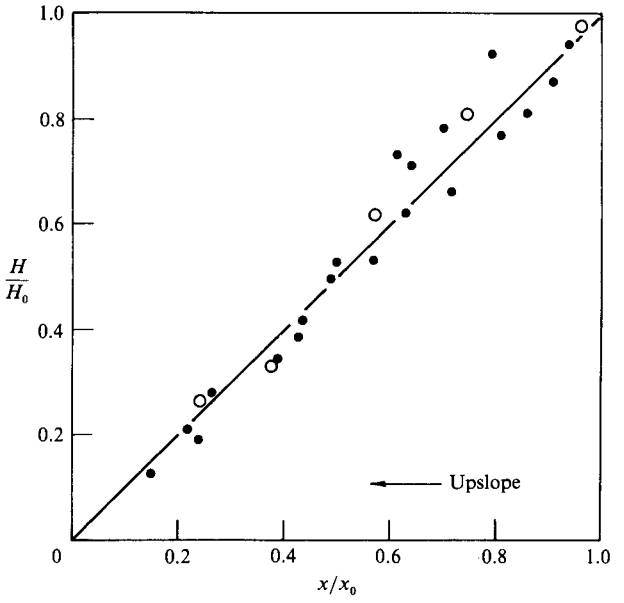

FIGURE 15. Normalized bolus height H/H_0 as a function of the normalized distance from the limit of run-up x/x_0. Bedslope: ●, $\theta = 0.030$; ○, $\theta = 0.054$.

where c_0 is the initial velocity of the bolus and

$$\phi = \frac{x_0}{H_0}\left(\frac{S_1 R_i \sin\theta + C_D}{S_1(1+k_v)}\right) - 2. \tag{11}$$

The characteristic density excess of the bolus can be determined by recognizing that R_i is constant, and it then follows from (8) and (10) that

$$\frac{A}{A_0} = \left(\frac{x}{x_0}\right)^{2\phi-1}. \tag{12}$$

The equation of motion dictates that a bolus, whose structure is self-preserving during the run-up phase, obeys simple power laws which determine its variation of height, celerity and density. Although the model predicts that the height of the bolus reduces linearly with distance from the break point, the celerity and density of the bolus vary at rates that depend on the slope and the coefficients of bolus area, added mass and drag.

The predictions of this simple model of bolus behaviour are now compared with observations of the height, celerity and density of the bolus during the run-up phase. Figure 15 shows the variation of bolus height expressed as a fraction of its initial height H_0 following the breaking event, expressed in terms of the normalized distance from the limit of run-up (x/x_0). The data compare favourably with the linear reduction in height predicted by the model.

Figures 16 and 17 show the variation of the vortex celerity and characteristic density excess as functions of the normalized distance from the limit of run-up. Both variables are normalized with respect to their values immediately following the breaking event. The curves in figures 16 and 17 are plots of the relevant theoretical relationship ((10) and (12) respectively) for ϕ-values of 0.6 and 0.8, which effectively span the data sets. The data for boluses on the steeper slope ($\theta = 0.054$) tend towards

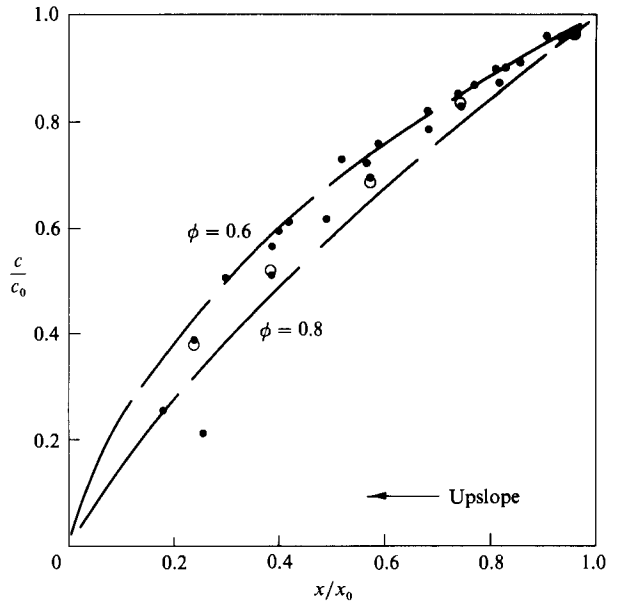

FIGURE 16. Normalized bolus celerity c/c_0 as a function of the normalized distance from the limit of run-up x/x_0. Bedslope: ●, $\theta = 0.030$; ○, $\theta = 0.054$.

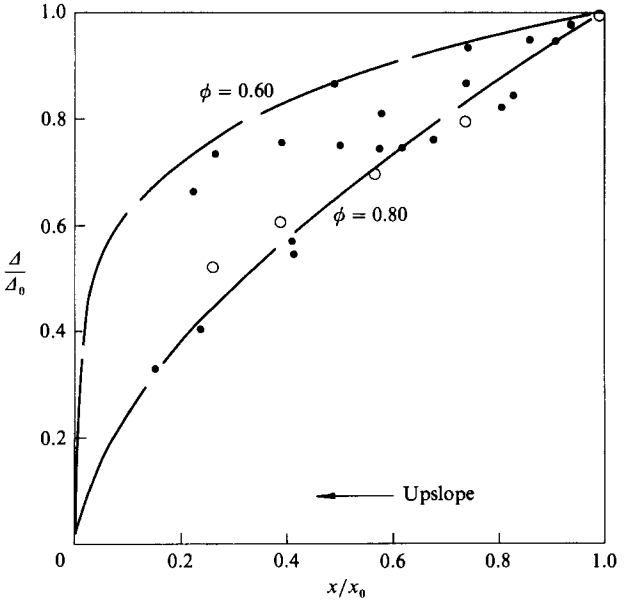

FIGURE 17. Normalized density excess within the bolus A/A_0 as a function of the normalized distance from the limit of run-up x/x_0. Bedslope: ●, $\theta = 0.030$; ○, $\theta = 0.054$.

larger values of ϕ while boluses on the lesser slope ($\theta = 0.030$) tend to have a smaller value of ϕ. This tendency is in accord with the relationship obtained for ϕ, (11), which suggests that ϕ increases with increasing θ.

It will be noted that the variation of the characteristic density with phase of run-up shows a much greater sensitivity to ϕ than does the celerity of the bolus. This is also reflected in the relative scatter of the experimental data in figures 16 and 17.

θ	0.030	0.054
x_0/H_0	33 ± 1	18.5 ± 1
S_1	2.4 ± 0.2	1.9 ± 0.2
R_i	1.27 ± 0.34	2.4 ± 0.3
k_v	0.65 ± 0.05	0.80 ± 0.10
C_D	0.22 ± 0.03	0.25 ± 0.04
ϕ (eq. (11))	0.60 ± 0.37	0.68 ± 0.24
ϕ (experiment)	0.60 ± 0.05	0.66

TABLE 1. Values of the index ϕ based on (11) compared with values based on the observed variation of bolus celerity and density excess during run-up

Data from all of the six experiments are shown in figures 15, 16 and 17. ϕ was found to have a mean value of 0.60 ± 0.05 for the slope of 0.030 and a value of 0.66 for the single experiment on a slope of 0.054.

It is interesting to compare these values for ϕ with values determined from (11) where ϕ was shown to be a function of the run-up ratio x_0/H_0, bedslope θ, bolus shape parameter S_1, Richardson number R_i, added-mass coefficient k_v and drag coefficient C_D. All of these parameters with the exception of the last two, could be measured directly from the experiments. k_v was estimated using a semi-ellipse with the ratio of the minor to major axes set to the appropriate value of $2H/L$. The drag coefficients were estimated using data from the study by Simpson & Britter (1979) of the structure of gravity-current heads. The calculation is lengthy and was based on equating the rate of energy dissipation associated with the motion of the head to the rate of work done against the drag force exerted by the flow on the head. Details of the calculation are given by Wilkinson (1983).

Table 1 lists the estimated values of the parameters in (11) obtained by the means described above and gives the values of ϕ based on these figures. Agreement between the observed and predicted values of ϕ are remarkably close in view of the large relative error in the calculated values.

3.3. *Energetics*

The propagation of internal waves onto the slope involved several mechanisms of energy transformation: (*a*) reflection of incident wave energy by the slope; (*b*) turbulence production leading to dissipation of kinetic energy and a gain in potential energy produced by the mixing; and (*c*) work done against bottom stresses.

The energy reflected from the slope was not detectable with the available instrumentation, indicating that it was less than 3% of the incident-wave energy. The energy dissipation that occurred after the overturning event can be examined by considering the kinetic and potential energy of the bolus relative to a datum set at the breakpoint and is given by

$$E = \tfrac{1}{2}\rho S_1(k_v+1)H^2c^2 + [\tfrac{1}{2}H + (x_0-x)\sin\theta]S_1\Delta\rho g H^2. \tag{13}$$

The rotational energy and turbulent kinetic energy of the bolus were not included in (13), however, because with the self-preserving nature of the bolus both would scale in direct proportion to the kinetic energy of translation. Analysis of motion-picture recordings of neutrally buoyant particles within the bolus showed that the rotational energy was an order of magnitude less than the kinetic energy of translation and that the kinetic energy of turbulent motions was significantly less again. If the energy of

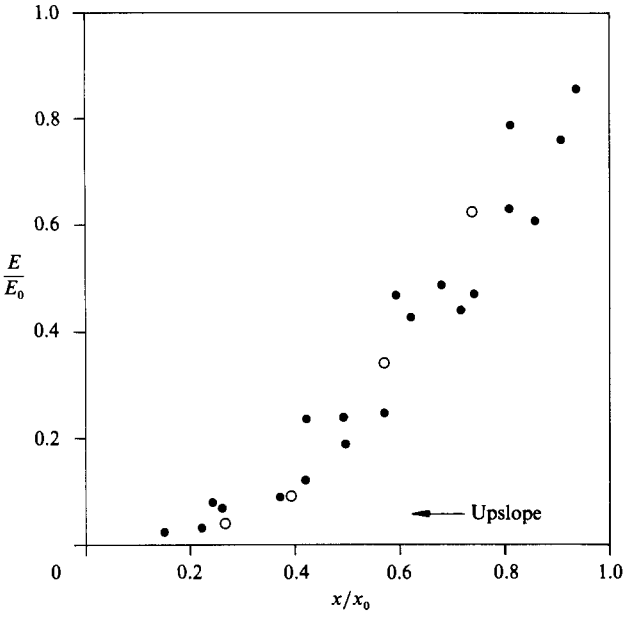

FIGURE 18. Normalized energy of the bolus E/E_0 as a function of the normalized distance from the limit of run-up x/x_0. Bedslope: ●, $\theta = 0.030$; ○, $\theta = 0.054$.

the bolus E is normalized with respect to its initial energy at the datum E_0, the following results:

$$\frac{E}{E_0} = \left(\frac{cH}{c_0 H_0}\right)^2 \frac{1+k_v+\left[\frac{2(x_0-x)}{H}\sin\theta+1\right]R_i}{1+k_v+R_i}. \tag{14}$$

E/E_0 was calculated at various stages of run-up in all six experiments and is plotted against x/x_0 in figure 18.

The trend was similar in all of the experiments and showed an initially rapid rate of dissipation with approximately 80% of the energy being dissipated over the first half of the run-up. The dissipation indicated in figure 18 includes the rotational and turbulent kinetic energy of the bolus, the work done against bottom friction and the total energy of the backflow between the point of overturning and the section of interest.

The mixing associated with the turbulent dissipation of kinetic energy resulted in an increase in the potential energy of the system viewed as a whole. This transformation, together with the reflected-wave energy, were the only mechanisms by which mechanical energy was conserved. The remaining incident energy was ultimately converted to heat. It is of interest to examine the fraction of incident-wave energy flux that is recovered as a gain in the potential energy of the system. The gain in potential energy occurred by drainage of the mixed backflow down the slope and out along the original interface.

Each bolus carried a volume $S_1 H_0^2$ of dense fluid onto the slope where it mixed with lighter fluid and eventually drained back to form the intrusive layer along the original interface. The depth of the intrusive layer was approximately one tenth of the initial wave height and the centroid of its density excess was located about one third of the layer thickness above its base. Therefore the gain in potential energy of

the system produced by unit volume of backflow amounted to $\frac{1}{30}\Delta_0 \rho g H$ so that each wave increased the potential energy of the system by

$$\delta V = \frac{\Delta_0 \rho g H_0}{30} S_1 H_0^2.$$

There was no evidence of strong energy dissipation until after the bolus had formed so that the initial energy may be taken from (13) to give

$$E_0 = \tfrac{1}{2}\rho S_1[(k_v + 1) H_0^2 c_0^2 + \Delta_0 g H_0^3].$$

The ratio of potential-energy gain to the initial wave energy is given by

$$\frac{\delta V}{E_0} = \frac{R_i}{15(1 + k_v + R_i)},$$

which in these experiments amounted to about 3%. Thus relatively little of the incident-wave energy was recovered as an increase in the potential energy of the system.

4. Conclusions

The interaction of periodic interfacial gravity waves with a gentle slope in a system composed of two miscible layers has been described. Away from the slope the incident waves were long and of small amplitude and the oscillatory motions were very nearly sinusoidal. As the waves progressed onto the slope they steepened and developed into a train of solitary-like waves. Ultimately the solitary waves became kinematically unstable and this resulted in an overturning which led to a collapse of the wave and the formation of a turbulent bolus. The overturning was accompanied by the engulfment of ambient fluid causing the density excess of the bolus to be less than that of the internal wave from which it evolved. The bolus was characterized by a strong vertical motion and internal mixing. It was found that the height and density excess of the bolus when it first evolved relative to a characteristic wavelength and density excess of the incident wave was determined by a characteristic energy-flux parameter based on conservative properties of the wave. Within a distance of several wave heights from the point of overturning, the structure of the bolus was found to stabilize and to then remain unchanged during the subsequent run-up. Dense fluid was transported up the slope in the bolus and there was continuous drainage of dense fluid from the rear of the bolus causing its volume to slowly diminish as it progressed up the slope. Thus each bolus advanced into a shallow counterflow which was composed of the backflow from previous boluses. The density excess within the bolus also reduced as it travelled upslope due to entrainment from the backflow and surrounding fluid.

A bulk Richardson number based on the characteristic density excess of a bolus, its height and speed, was found to remain constant over much of the run-up, confirming the self-preserving nature of this phase. The self-preserving property was employed in a simple model which showed that the parameters characterizing the bolus could be expressed in terms of power laws involving a normalized run-up distance.

Once a bolus formed the incident-wave energy was rapidly dissipated. Mixing during its dissipative phase produced some increase in the potential energy of the system; however this amounted to only about 3% of the incident-wave energy.

The authors would like to express their appreciation to the Royal Australian Navy for providing the facilities used to obtain the information shown in figure 1. We would also like to thank one of the reviewers for a substantial and constructive criticism of the original draft of this paper.

Appendix A

Experiment no.	d_ℓ	d_u	d	Δ_ℓ	T	λ	H_w	c
1	125	375	94	0.047	18.9	3760	7.2	200
2	125	375	94	0.041	18.9	3110	11.5	165
3	130	370	96	0.048	6.33	1160	9.8	185
4	130	370	96	0.051	18.9	3650	20.6	195
5	130	370	96	0.013	18.8	2050	15.5	110
6	135	365	99	0.051	18.8	4090	8.4	220

TABLE 2. Summary of the data relating to the incident wave in the constant-depth section of the tank. All lengths are given in mm and all times in s. Here d_ℓ = depth of the lower layer; d_u = depth of the upper layer; $d = d_u d_\ell/(d_u+d_\ell)$; Δ_ℓ = difference in relative density of the upper and lower layers; T = wave period; λ = wavelength; H_w = wave height; c = wave celerity.

Experiment no.	θ	H_0	c_0	Δ_0	x_0
1	0.030	36	79	0.0215	1100
2	0.030	43	85	0.0260	1580
3	0.030	32	77	0.0305	880
4	0.030	62	109	0.0260	2300
5	0.030	38	47	0.0100	1150
6	0.054	58	71	0.0220	1220

TABLE 3. Summary of the data relating to the bolus. All lengths are given in mm and all times in s. Here θ = bedslope in rad; H_0 = wave height at breaking (initial formation of bolus); c_0 = wave celerity at breaking; Δ_0 = density excess in bolus at breaking; x_0 = total run-up distance of bolus.

Appendix B. The characteristic energy flux P^* and wave steepness a_0/λ_0

Here, the relationship between the characteristic energy flux P^* of an internal wave and the steepness of the same wave when the layer depths to either side of the interface are large is examined.

The energy flux P is a conservative quantity and is given by

$$P = \tfrac{1}{2}\Delta g a^2 c_g.$$

When both layers are deep, the group velocity c_g is equal to half the phase speed of an interfacial wave, so that

$$c_g = \lambda_0/2T = \Delta g T/4\pi,$$

where λ_0 is the reference wavelength defined in (2).

The characteristic energy flux P^* is defined as

$$P^* = PT^3/\lambda_0^4,$$

which, after substituting for Δg and c_g, gives

$$P^* = \tfrac{1}{2}\pi (a_0/\lambda_0)^2,$$

in which a_0 is the wave amplitude corresponding to the wavelength λ_o. The characteristic energy flux P^* is therefore proportional to the square of the wave steepness (a_0/λ_0) when the layers are deep.

REFERENCES

ALONSO, C. V. 1971 Comparative study of electrical conductivity probes. *J. Hydraul. Res.* **9**, 1–10.

BAINES, P. G. 1982 On internal tide generation models. *Deep-Sea Res.* **29**, 307–338.

CACCHIONE, D. A. & WUNSCH, C. 1974 Experimental study of internal waves over a slope. *J. Fluid Mech.* **66**, 223–239.

DAVIS, R. E. & ACRIVOS, A. 1967 Solitary internal waves in deepwater. *J. Fluid Mech.* **29**, 593–607.

DJORDJEVIC, V. D. & REDEKOPP, L. G. 1978 The fissional disintegration of internal solitary waves moving over 2-dimensional topography. *J. Phys. Oceanogr.* **10**, 813–819.

EMERY, K. O. & GUNNERSON, C. G. 1973 Internal swash and surf. *Proc. Nat. Acad. Sci.* **70**, 2379–2380.

ERIKSEN, C. C. 1982 Internal wave reflection off slopes. *J. Geophys. Res.* **87**, 525–538.

GODA, Y. 1970 A synthesis of breaker indices. *Trans. Japan Soc. Civ. Engrs* **2**, 39–49.

HALL, J. M. & PAO, Y.-H. 1969 Spectra of internal waves and turbulence in stratified fluids. Part 2. *Radio Sci.* **4**, 1321–1325.

HAURY, L. R., BRISCOE, M. G. & ORR, M. H. 1979 Tidally generated internal wave packets in the Massachusetts Bay. *Nature* **278**, 312–317.

HELFRICH, K. R. & MELVILLE, W. K. 1986 On long internal waves over slope–shelf topography. *J. Fluid Mech.* **167**, 285–308.

JONES, I. S. F. & PADMAN, L. 1983 Semidiurnal internal tides in Eastern Bass Strait. *Austral. J. Mar. Freshwat. Res.* **34**, 159–171.

KAO, T. W., PAN, F.-S. & RENOUARD, D. 1985 Internal solitons on the pycnocline generation, propagation, shoaling and breaking over a slope. *J. Fluid Mech.* **159**, 19–53.

MAXWORTHY, T. 1980 Gravitational collapse of mixed regions. *J. Fluid Mech.* **96**, 65–80.

MUNK, W. H. 1949 The solitary wave theory and its application to surf problems. *Ann. N. Y. Acad. Sci.* **51**, 376–462.

MUROTA, A., HIRATA, T. & MICHIOKU, K. 1980 Characteristics of internal gravity wave and its breaking on sloping bed. *Trans. Japan Soc. Civ. Engrs, Hyd. San. Engng Div.* **12**, 149–150.

NAGASHIMA, H. 1971 Reflection and breaking of internal waves on a sloping beach. *J. Oceanogr. Soc. Japan* **27**, 1–6.

OSBORNE, A. R. & BURCH, T. L. 1980 Internal solitons in the Andaman Sea. *Science* **208**, 451–459.

PEREGRINE, H. W. 1974 Surface shear waves. *J. Hydraul. Div., ASCE*, HY9, 1215–1227.

PINGREE, R. D. & MARDELL, G. T. 1981 Slope turbulence, internal waves and phytoplankton growth at the Celtic Sea shelf-break. *Phil. Trans. R. Soc. Lond.* A **302**, 663–682.

SIMPSON, J. E. 1972 Effects of the lower boundary on the head of a gravity current. *J. Fluid Mech.* **53**, 759–768.

SIMPSON, J. E. & BRITTER, R. E. 1979 The dynamics of the head of a gravity current advancing over a horizontal surface. *J. Fluid Mech.* **94**, 477–495.

SOUTHARD, J. B. & CACCHIONE, D. A. 1972 Experiments on bottom sediment movement by breaking internal waves. In *Shelf Sediment Transport: Process and Pattern* (ed. D. J. P. Swift, D. B. Duane & P. H. Pilkey), chap. 4. Dowden, Hutchinson & Ross.

THORPE, S. A. 1966 Internal gravity waves. Ph.D. dissertation, University of Cambridge.

WILKINSON, D. L. 1983 Studies into the structure and motion of density currents. *University of New South Wales, Water Res. Lab. Rep.* 160.

WOOD, I. R. & SIMPSON, J. E. 1984 Jumps in layered miscible fluids. *J. Fluid Mech.* **140**, 329–342.